Available online at www.sciencedirect.com

ScienceDirect

Palaeoworld 35 (2026) 201049

Palaeoworld

www.elsevier.com/locate/palwor

Fossil sardines from the Pisco Formation (Miocene), Peru: Taxonomy, taphonomy, and paleoecology

Giorgio Carnevale [a,*], Luca Pellegrino [a], Giulia Bosio [b], Giovanni Bianucci [b], Alberto Collareta [b], Claudio Di Celma [c], Elisa Malinverno [d], Abel Alejandro Ramirez Ampuero [e], Luz Tejada-Medina [f], César Chacaltana [f], Mario Urbina [e], Giuseppe Marramà [a]

[a] *Dipartimento di Scienze della Terra, Università degli Studi di Torino, Torino, Italy*
[b] *Dipartimento di Scienze della Terra, Università di Pisa, Pisa, Italy*
[c] *Scuola di Scienze e Tecnologie, Università di Camerino, Camerino, Italy*
[d] *Dipartimento di Scienze dell'Ambiente e della Terra, Università di Milano-Bicocca, Milano, Italy*
[e] *Universidad Nacional Mayor de San Marcos (UNMSM), Lima, Peru*
[f] *Instituto Geológico, Minero y Metalúrgico (INGEMMET), Lima, Peru*

Received 10 June 2025; received in revised form 24 October 2025; accepted 5 November 2025
Available online 9 November 2025

Abstract

The Miocene sedimentary sequences of the Pisco Formation (Eastern Pisco Basin, southern Peru) are renowned for the abundance of fossil vertebrates that document the early evolution of the biotic communities of the Humboldt Current Ecosystem. Vertebrate remains are often exceptionally preserved, representing a variety of fishes, turtles, crocodiles, birds, and marine mammals. Here, we describe a new species of sardine, *Sardinops humboldti* n. sp., based on partially complete articulated skeletons from the Upper Miocene P2 sequence of the Pisco Formation. This new species is morphologically similar to the extant Indian-Pacific species *S. sagax* from which it differs by having larger parietals, a thick and much elongate supraoccipital crest, anterolateral processes of the sphenotics that protrude obliquely from the skull roof, posterior margins of the supraoccipital and epioccipitals forming a broad acute angle approaching 90°, and gently rounded ventral margin of the opercle. Taphonomic and paleoecological evidences suggest that *S. humboldti* n. sp. was probably very abundant in the Eastern Pisco Basin where it formed relatively small schools of large individuals that were uniform in size, representing the trophic nucleus of the diverse vertebrate communities. Paleobiogeographic implications are also discussed.

Keywords: Teleostei; *Sardinops humboldti* n. sp.; paleobiogeography

1. Introduction

The Pisco Formation is a Neogene sedimentary unit broadly exposed in the East Pisco Basin (EPB), southern Peru. The Miocene deposits of the Pisco Formation are globally renowned for their abundant remains of marine vertebrates, which include a variety of odontocete and mysticete cetaceans, seals, seabirds, crocodiles, turtles, and bony and cartilaginous fishes (e.g., Bosio et al., 2021; Collareta et al., 2021). Overall, the fossil vertebrate assemblages of the Pisco Formation offer a unique deep-time perspective of the evolution of the biotic communities of the Humboldt Current Ecosystem (Collareta et al., 2021).

* Corresponding author.
E-mail address: giorgio.carnevale@unito.it (G. Carnevale).

https://doi.org/10.1016/j.palwor.2025.201049
1871-174X/

The evolutionary paleoecological scenario depicted by Collareta et al. (2021) for the Pisco Formation hypothesized a complex ecosystem driven by upwelling and supported by abundant schools of epipelagic fishes. However, while the diversity and paleobiological significance of marine mammals, seabirds, and cartilaginous fishes of the Pisco Formation have been extensively investigated (e.g., Bianucci et al., 2016; Collareta et al., 2021; Bianucci and Collareta, 2022), the structure and composition of the bony fish communities remain largely elusive. In particular, the identity of the sardines, whose prominent ecological role in the Pisco Basin has been evidenced by recent studies (Collareta et al., 2015, 2017, 2021; Lambert et al., 2015), is still uncertain. Despite sardine remains have been reported in regurgitates or stomach contents of fossil odontocete and mysticete cetaceans from the Pisco Formation (Collareta et al., 2015; Lambert et al., 2015), skeletal remains of these fishes are rather uncommon elsewhere. Recent field activities in the Ocucaje area, near the site of Las Antenas, however, led to the discovery of relatively abundant sardine skeletal remains. The goal of this paper is therefore to describe these fossil sardines and to discuss their taxonomic status, taphonomic features, and paleoecological significance.

2. Geological and stratigraphic setting

The Peruvian margin is shaped by the subduction of the Nazca Plate beneath South America, resulting in a predominantly erosive convergent margin (Clift and Vannucchi, 2004; Noda, 2016). The forearc is segmented into trench-parallel basins by the Outer Shelf High, a structural ridge of Precambrian–Paleozoic basement. In southern Peru, the onshore EPB (Fig. 1A) and the offshore West Pisco Basin are separated by the uplifted Coastal Cordillera (Romero et al., 2013), reflecting a complex history of uplift and subsidence driven by plate interaction (von Huene and Suess, 1988; Herbozo et al., 2020) and the subduction of the aseismic Nazca Ridge (Hsu, 1992; Macharé and Ortlieb, 1992). The EPB preserves a well-exposed Cenozoic marine sedimentary succession, from the oldest Paracas Formation to the youngest Pisco Formation (Dunbar et al., 1990). In the Ica River Valley, the latter spans from Middle to Late Miocene and is subdivided into three sequences (P0, P1, P2), each bounded by regional unconformities (PE0.0, PE0.1, PE0.2) (Di Celma et al., 2022).

At the Las Antenas locality (Fig. 1B), also known as Cerro Pileta (Tejada et al., 2010), the uppermost exposed

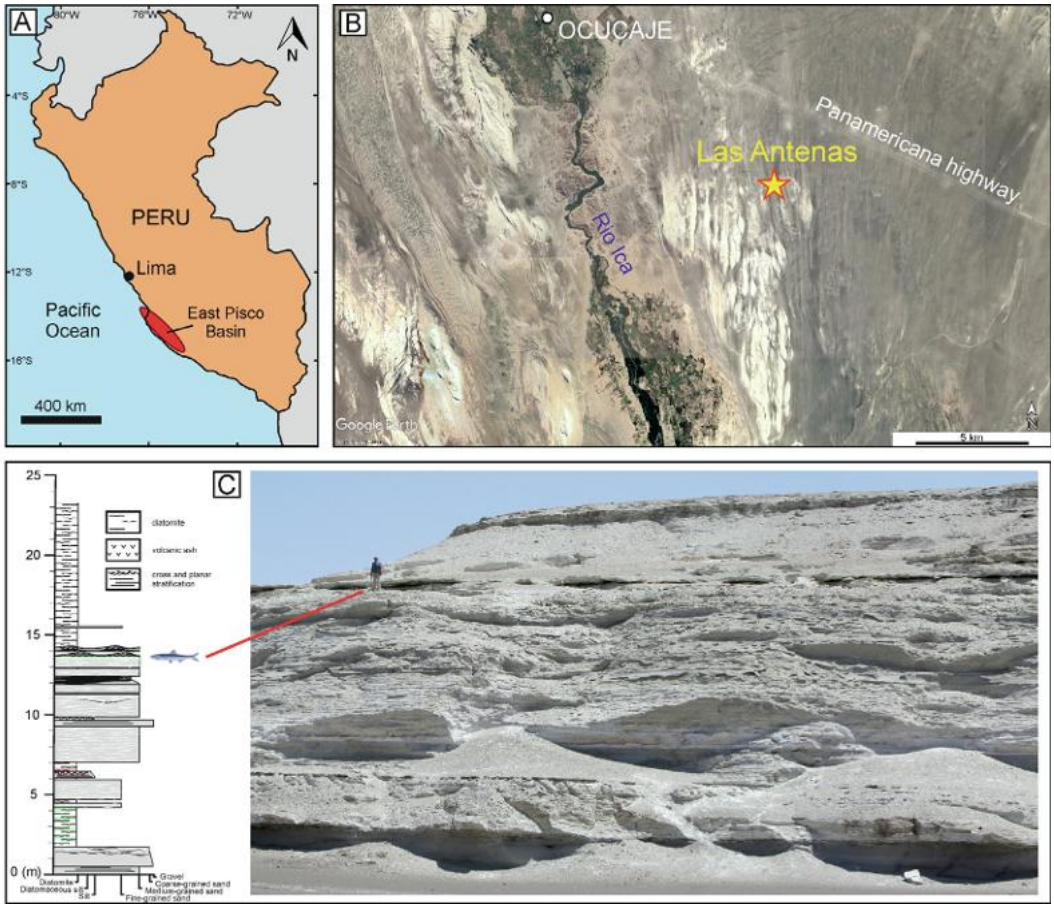

Fig. 1. (A) Geographic location of the East Pisco Basin along the Peruvian coast. (B) Satellite image of the locality of Las Antenas (Ica Desert, Peru) based on Google Earth. (C) Measured stratigraphic log and outcrop view of the Pisco (P2) deposits at the locality of Las Antenas, with indication of the sardine-rich horizon.

portion of the Pisco Formation — corresponding to the P2 sequence (8.4 to ≥ 6.71 Ma in age; Di Celma et al., 2022) — occurs. This unit comprises diatomites, siltstones, volcanic ashes, and fine- to coarse-grained sandstones, and is characterized by predominant hummocky cross-stratification and sporadic ripple cross-lamination, small pebble lenses and gutter casts (Fig. 1C). The sedimentary structures and grain sizes indicate deposition in the offshore transition zone, under the influence of high-energy storm events and combined flows near the storm-wave base (Bosio et al., 2021). Within this section, a layer enriched in sardine skeletal remains is present (GPS coordinates of the main outcrop: 14°26'06.9''S, 75°34'46.1''W) (Fig. 1B, C). The same horizon has been recognized some 800 m SSE from the main outcrop (14°26'32.2''S, 75°34'34.8''W). Most of the fossil material analyzed in this study was recovered from this horizon.

3. Materials and methods

The present study is based on 55 specimens deposited in the Museo de Historia Natural de la Universidad Nacional Mayor de San Marcos (MUSM), Lima, Peru. The fossil remains were found embedded within friable white-greenish diatomites alternated to sandstones pertaining to the P2 sequence (Fig. 1C). Most of the specimens were collected during field work in September 2022 and January 2024 from the main outcrop and consist of isolated incomplete neurocrania and other head bones, and incomplete articulated vertebral columns. In addition, a few specimens were collected from the same horizon ca. 800 m SSE of the main outcrop; these consist of articulated or associated postcranial remains preserved within nodules. Finally, isolated or associated scales have been collected from finely laminated diatomites just above the more massive diatomite that yielded the skeletal remains. The specimens required matrix removal before examination; this was achieved using fine entomological needles. These were examined for morpho-anatomical purposes using a Leica M80 stereomicroscope equipped with a camera lucida drawing arm. Two specimens, one isolated and one embedded in a nodule, were selected for in-depth petrographic investigations in light and scanning electron microscopy (SEM). After preliminary observations of specimens in reflected light (Leica Microsystems), polished thin sections were prepared and subsequently observed in transmitted light with an optical microscope equipped with digital camera (Leica Microsystems). Then, sections were carbon-coated and observed with a SEM in backscattered electron (BSE) mode, coupled with electron dispersive X-ray spectroscopy (EDS) for semi-quantitative elemental analyses (JSM IT300LV, JEOL Limited). In addition, some freshly broken chips were obtained from small portions of the nodule, gold-coated and analyzed with SEM-EDS both in BSE and secondary electron (SE) mode (Tescan Vega, Tescan).

4. Systematic paleontology

Order Clupeiformes Bleeker, 1859
Family Alosidae Svetovidov, 1952
Genus *Sardinops* Hubbs, 1929

Sardinops humboldti Carnevale and Marramà n. sp.
(Figs. 2–4, 6, 7)

2015 *Sardinops* sp. cf. *S. sagax* (Jenyns) – Collareta et al., p. 6, text-figs. 4–6.
2015 *Sardinops* sp. cf. *S. sagax* (Jenyns) – Lambert et al., p. 4, text-fig. 2.
2017 *Sardinops* sp. cf. *S. sagax* (Jenyns) – Collareta et al., p. 15, text-fig. 2.
2021 *Sardinops* sp. cf. *S. sagax* (Jenyns) – Oyanadel-Urbina et al., p. 349, text-fig. 2.

Etymology: Species named after the German naturalist, explorer and geographer Friedrich Heinrich Alexander Freiherr von Humboldt.
Holotype: MUSM 4724, a partially complete neurocranium, lacking the ethmoid portion (Fig. 2).
Paratypes: MUSM 4728, a partially complete neurocranium, lacking the ethmoid portion (Fig. 3A); MUSM 4726, a partially complete neurocranium, lacking the ethmoid portion (Fig. 3B); MUSM 4738, a partially complete neurocranium, lacking the ethmoid portion (Fig. 3C); MUSM 4737, a partially complete neurocranium, lacking the ethmoid portion (Fig. 3D); MUSM 4730, a partially complete neurocranium, lacking the ethmoid portion, with associated branchial skeleton and anterior part of the axial skeleton (Fig. 3E, F); MUSM 4725, a partially complete neurocranium, lacking the ethmoid portion (Fig. 3G); MUSM 4723, a partially complete neurocranium, lacking the ethmoid portion (Fig. 3H); MUSM 4735, a partially complete neurocranium, lacking the ethmoid portion (Fig. 3I); MUSM 4736, a partially complete neurocranium, lacking the ethmoid portion (Fig. 3J); MUSM 4727, a partially complete neurocranium, lacking the ethmoid portion (Fig. 3K); MUSM 4718, a largely incomplete neurocranium, lacking the ethmoid portion and most of the left side; MUSM 4719, a partially complete neurocranium, lacking the ethmoid portion; MUSM 4720, a partially complete neurocranium, lacking the ethmoid portion; MUSM 4731, a partially complete neurocranium, lacking the ethmoid portion, in part and counterpart (Fig. 4); MUSM 4721, incomplete left opercle and subopercle (Fig. 6A); MUSM 4732, a partially complete left opercle; MUSM 4722, a partially complete neurocranium, lacking the ethmoid portion, articulated with an incomplete abdominal portion of the vertebral column (Fig. 6B); MUSM 4717, two largely incomplete articulated vertebral columns with associated intermuscular bones (Fig. 6C), and articulated pelvic scutes (Fig. 5D); MUSM 4739, isolated scales (Fig. 6E); MUSM 4733, a partially complete preural por-

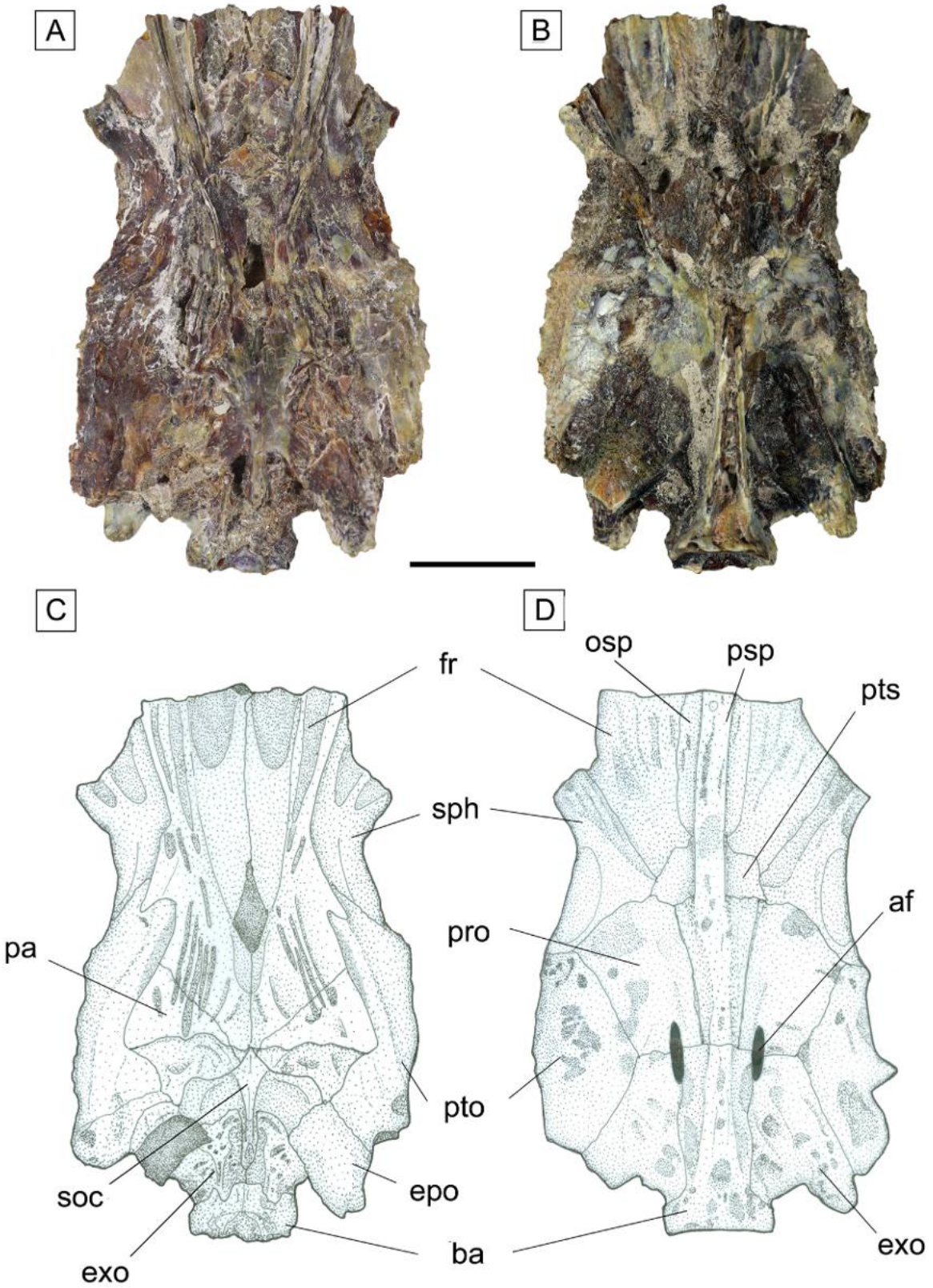

Fig. 2. *Sardinops humboldti* n. sp. from the Upper Miocene of Las Antenas, Pisco Formation, Peru. (A, B) Holotype, MUSM 4724, in dorsal (A) and ventral (B) view. (C, D) Reconstruction of the holotype, MUSM 4724, in dorsal (C) and ventral (D) view. Scale bar = 10 mm. Abbreviations: af, auditory fenestra; ba, basioccipital; epo, epioccipital; exo, exoccipital; fr, frontal; pa, parietal; osp, orbitosphenoid; pro, prootic; psp, parasphenoid; pto, pterotic; pts, pterosphenoid; soc, supraoccipital; sph, sphenotic.

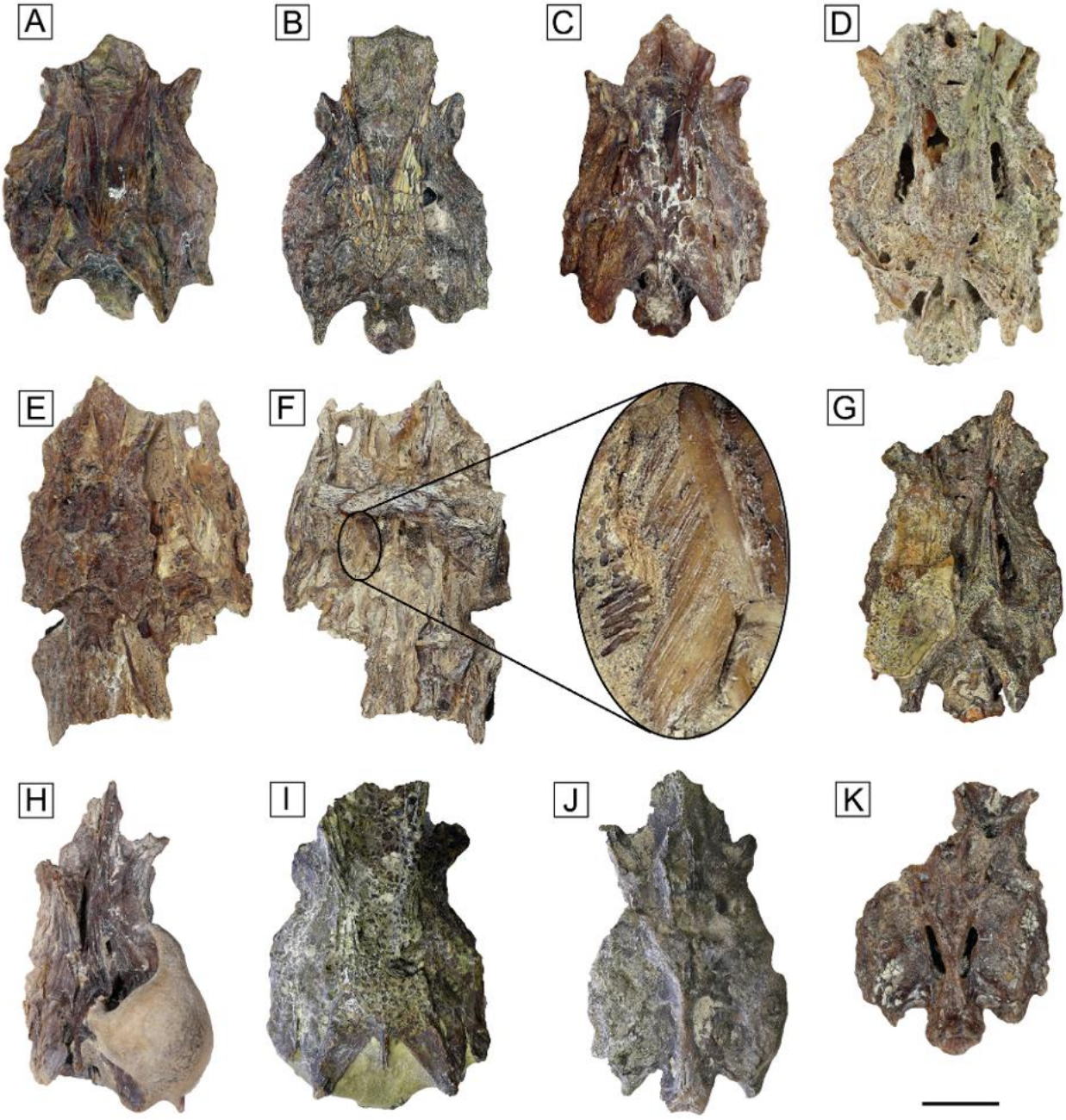

Fig. 3. *Sardinops humboldti* n. sp. from the Upper Miocene of Las Antenas, Pisco Formation, Peru. (A–K) Neurocrania of selected paratypes; (A) MUSM 4728, dorsal view; (B) MUSM 4726, dorsal view; (C) MUSM 4738, dorsal view; (D) MUSM 4737, dorsal view; (E, F) MUSM 4730 in dorsal (E) and ventral (F) view with relative close up showing some gill rakers; (F) MUSM 4725, dorsal view; (G) MUSM 4725, dorsal view; (H) MUSM 4723, dorsal view; (I) MUSM 4735, dorsal view; (J) MUSM 4736, ventral view; (K) MUSM 4727, ventral view. Scale bar = 10 mm.

tion of the vertebral column, including the caudal skeleton (Fig. 7).

Type locality and horizon: Las Antenas; Pisco Formation; P2 sequence; Upper Miocene, Messinian.

Referred material: MUSM 4734, 34 incomplete neurocrania.

Diagnosis: A species of *Sardinops* characterized by large parietals, thick supraoccipital crest extending posteriorly over the anterior half of the exoccipitals; anterolateral processes of the sphenotics protruding obliquely from the skull roof; posterior margins of the supraoccipital and epioccipitals forming a broad acute angle approaching 90°; opercle with gently rounded ventral margin.

Description: All the available neurocrania are of similar size, somewhat dorsoventrally flattened due to taphonomic compression, and broken in the orbital region, lacking their ethmoid portion (Figs. 2–4). Therefore, the examined material actually consists of partially complete neurocrania

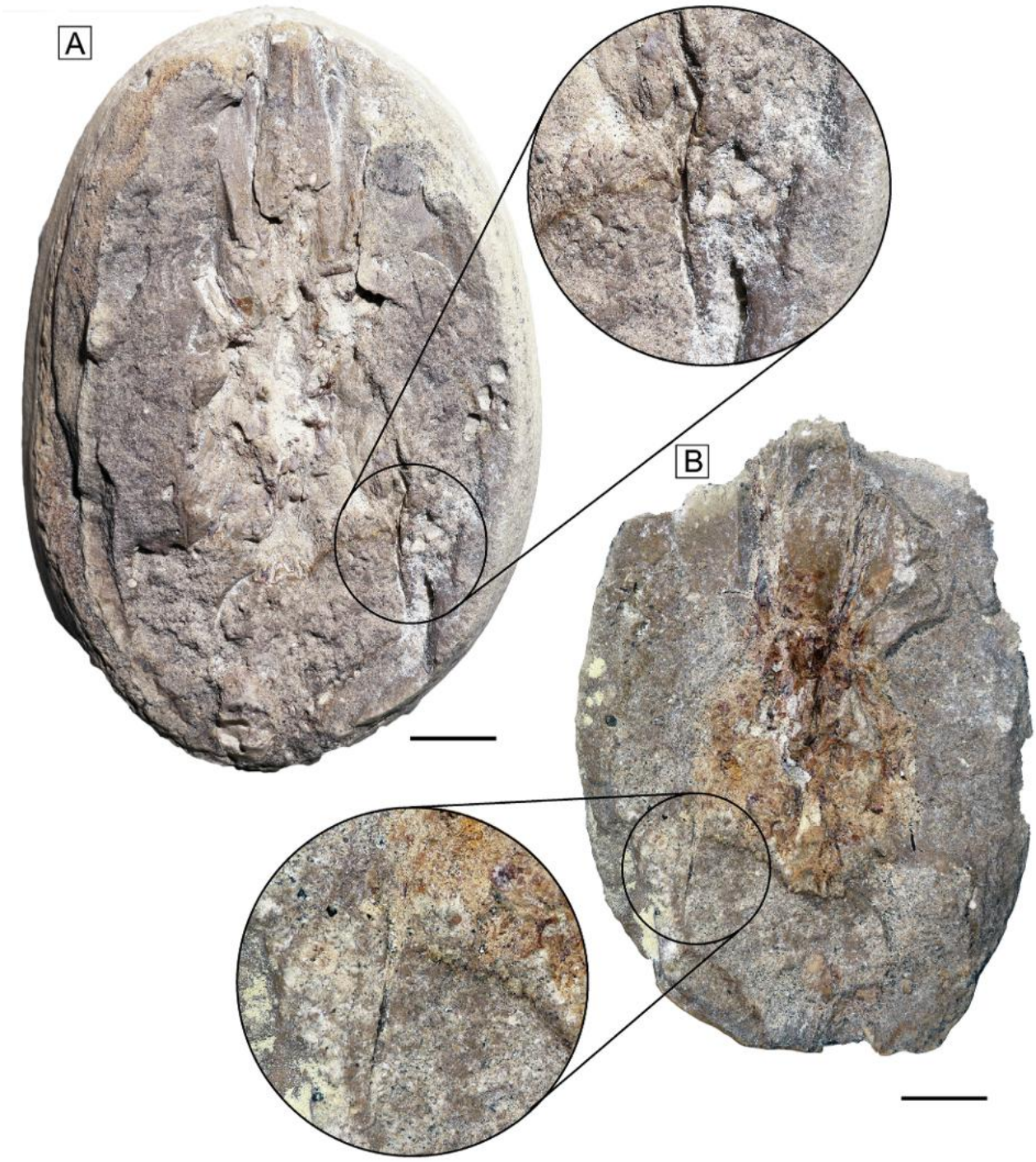

Fig. 4. *Sardinops humboldti* n. sp. from the Upper Miocene of Las Antenas, Pisco Formation, Peru. Paratype, MUSM 4731, in part (A) and counterpart (B) with close-up showing the pterotic spines. Scale bar = 10 mm.

represented by the posterior portion of the orbital region and almost complete postorbital region. Although the outer surface of the neurocranial bones is often slightly eroded, the overall structure of the neurocranium can be easily recognized and, especially the bony elements exposed in the basicranium, are extensively pitted with irregular pits. However, due to the taphonomic compression, the pre-epioccipital fossa and prootic and pterotic bullae (e.g., O'Connell, 1955) are largely obliterated and, consequently, their size and morphology are difficult to determine. However, a small pre-epioccipital fossa can be observed in MUSM 4737.

Overall, the available portion of the neurocranium is wedge-like, reaching the maximum width at the level of the pterotics. The frontals are the largest bones of the skull roof and articulate medially with each other through an

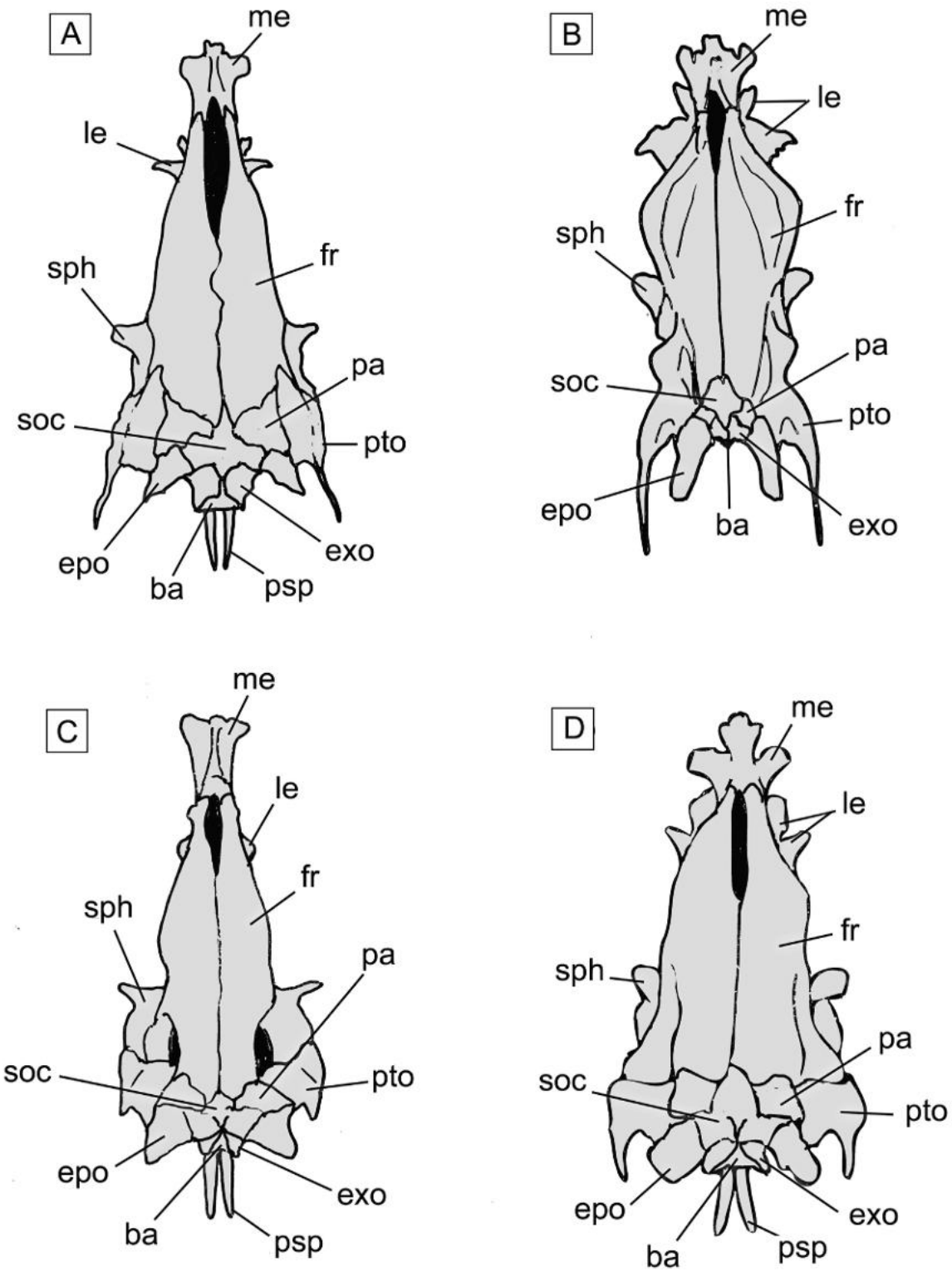

Fig. 5. Reconstructions of the skull roof in dorsal view of selected species of the four extant alosid genera. (A) *Sardinops sagax* (modified after Yabumoto, 1988). (B) *Brevoortia aurea* (modified after Segura and Díaz de Astarloa, 2004). (C) *Sardina pilchardus* (modified after Svetovidov, 1964). (D) *Alosa fallax* (modified after Svetovidov, 1964). Images not to scale. Abbreviations: ba, basioccipital; epo, epioccipital; exo, exoccipital; fr, frontal; le, lateral ethmoid; me, mesethmoid; pa, parietal; psp, parasphenoid; pto, pterotic; soc, supraoccipital; sph, sphenotic.

irregular suture. Each frontal gradually tapers anteriorly and has a prominent ridge characterized by well-defined longitudinal striations along its dorsal surface; these striations usually continue backward on the dorsal surface of the parietals. The medial portion of both the frontals is notably depressed, forming a longitudinal shallow fossa

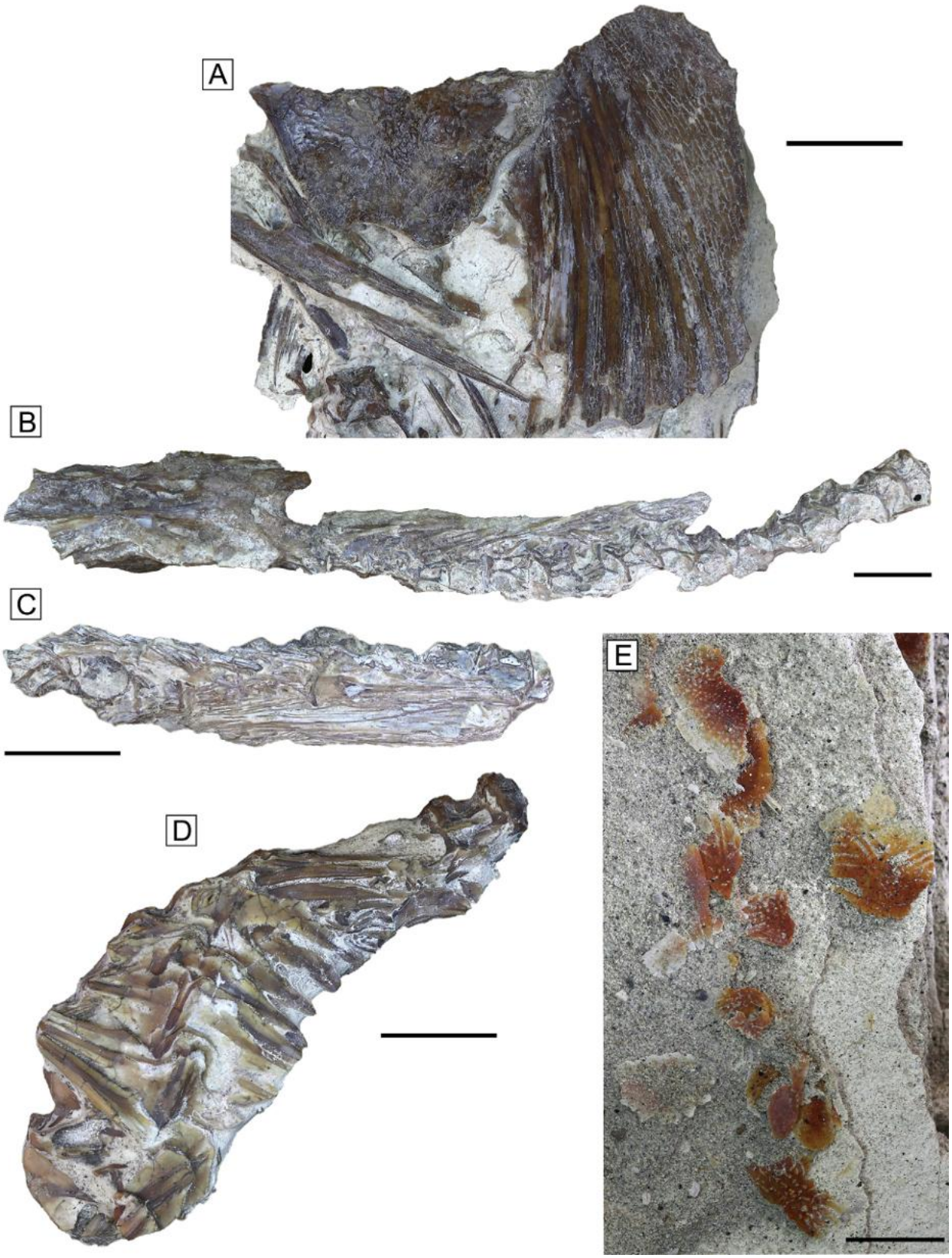

Fig. 6. *Sardinops humboldti* n. sp. from the Upper Miocene of Las Antenas, Pisco Formation, Peru. (A) Paratype, MUSM 4721, left opercle and subopercle. (B) Paratype, MUSM 4722, neurocranium articulated with an incomplete abdominal portion of the vertebral column. (C) Paratype, MUSM 4717, articulated vertebral columns with associated intermuscular bones. (D) Paratype, MUSM 4717, pelvic scutes. (E) Paratype, MUSM 4739, isolated scales. Scale bars = 10 mm.

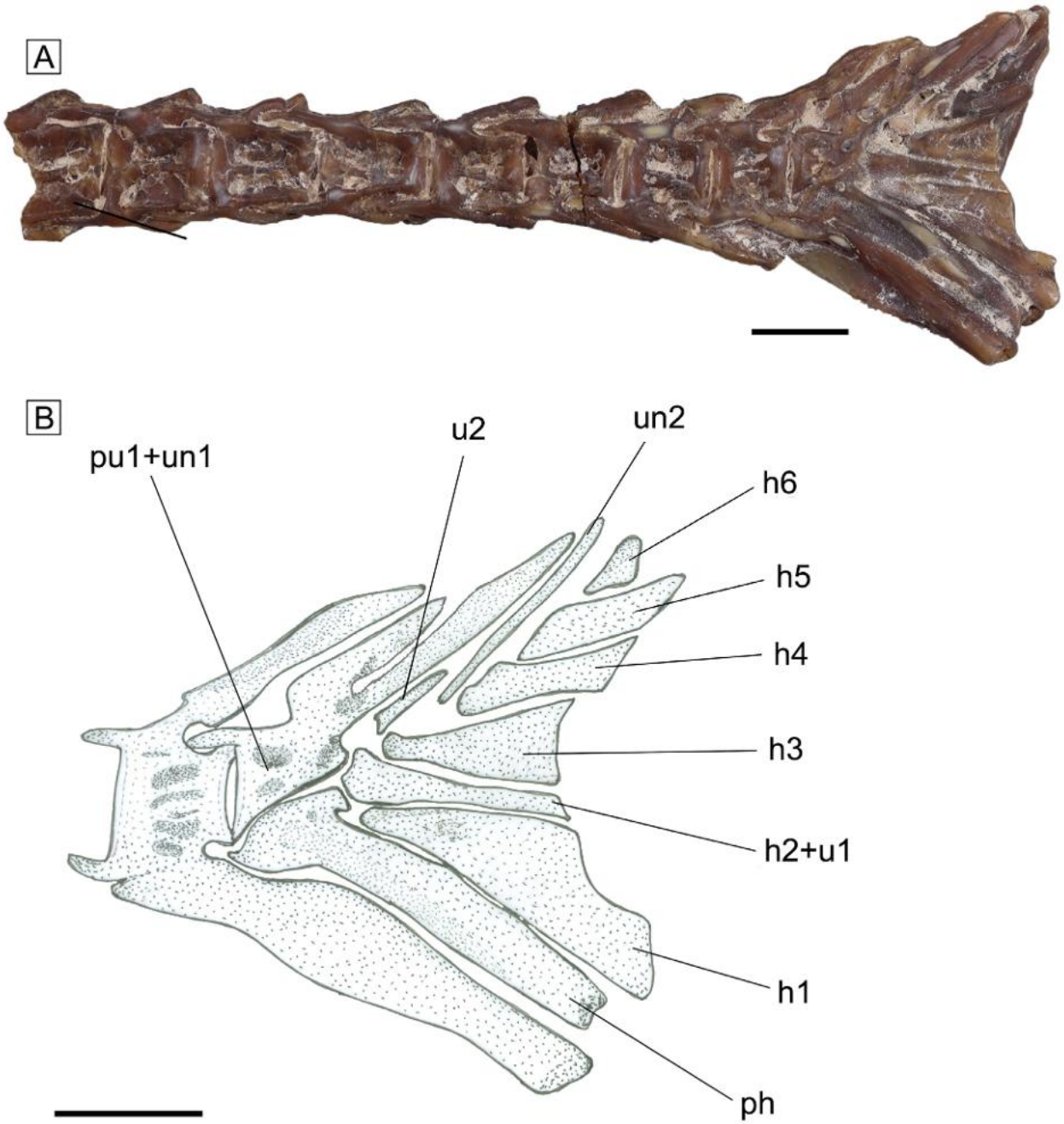

Fig. 7. *Sardinops humboldti* n. sp. from the Upper Miocene of Las Antenas, Pisco Formation, Peru; Paratype, MUSM 4733. (A) Left lateral view. (B) Reconstruction of the left lateral view of the caudal skeleton. Scale bars = 5 mm. Abbreviations: h, hypural; ph, parhypural; pu, preural centrum; u, ural centrum; un, uroneural.

sometimes associated to fontanelles at its extremities. Each frontal articulates posteriorly with the parietal, posteromedially with the supraoccipital, posterolaterally with the pterotic and sphenotic and ventromedially with the pterosphenoid and orbitosphenoid; the physical relationships with the mesethmoid and lateral ethmoids cannot be observed due to the inadequate preservation of the available material. The two paired parietals are irregular in shape, separated from each other by the supraoccipital, and definitely larger compared to those of the extant congeneric *Sardinops sagax* (Fig. 5A; see also Phillips, 1942; Svetovidov, 1952; Yabumoto, 1988). The supraorbital canal of the cephalic lateral-line system runs through the frontals and parietals. Each parietal articulates anteriorly with the frontal, medially and posteromedially with the supraoccipital, posteriorly with the epioccipital and laterally with the pterotic. The elongate temporal foramen is preserved in some specimens (e.g., MUSM 4722, MUSM 4737; see Fig. 3D), being shared by the frontals and parietals. The supraoccipital forms the upper median posterior apex of the neurocranium. It bears a thick and relatively low crest that extends posteriorly over the anterior half

of the exoccipitals, being considerably larger than that characteristic of *Sardinops sagax* (Fig. 5A; see also Phillips, 1942; Svetovidov, 1952; Yabumoto, 1988). The supraoccipital articulates anteriorly with the parietals, laterally with the epioccipitals and ventrally with the exoccipitals. The sphenotics are thick bones, each bearing a relatively large anterolateral process that protrudes obliquely from the skull roof, forming the posterodorsal wall of the orbit (Figs. 2, 3); these processes differ from those of the extant *S. sagax*, which are laterally directed, forming a right angle with the main axis of the neurocranium (Fig. 5A; see also Phillips, 1942; Svetovidov, 1952; Yabumoto, 1988). An oblong articular facet for the hyomandibula is clearly recognizable along its ventral surface. Each sphenotic articulates medially with the frontal, posteriorly with the pterotic, and ventromedially with the prootic and pterosphenoid. The pterotics are large and occupy most of the posterolateral region of the neurocranium. The posterolateral corner of the pterotics is commonly broken in the available specimens. However, a few specimens exhibit the conical posterior outline of these bones, which terminate posteriorly with a slender and pointed needle-like spinous process, extending longitudinally well beyond the posterior wall of the neurocranium (Fig. 4). The epioccipitals are stout and conical in outline, projecting posteriorly beyond the posterior wall of the neurocranium, to a considerably less extent of the needle-like pterotic process. The posterior margins of the supraoccipital and of each epioccipital form a broad acute angle approaching 90°; this condition is different from that characteristic of the extant *S. sagax* in which the posterior margins of these bones form an obtuse angle due to the more oblique direction of the projecting epioccipitals (see Svetovidov, 1952). The paired exoccipitals meet each other on the midline just below the supraoccipital. Their ventral side is characterized by a posterior conical process with a blunt distal end that protrudes from the rear of the neurocranium. Each exoccipital articulates dorsally with the supraoccipital, dorsolaterally with the epioccipital, ventromedially with the basioccipital, and anteroventrally with the prootic. Due to the inadequate preservation of the basicranium in the available material, it is difficult to recognize the intercalars and the basisphenoid. The basioccipital is massive and robust. It articulates anteriorly with the prootic and parasphenoid, and laterally and dorsally with the exoccipitals. An ovoid auditory fenestra, is recognizable bilaterally in certain specimens, enclosed by the basioccipital, exoccipitals and prootics (Figs. 2B–D, 3K). The prootic appears to be rather large and polygonal in outline. Each of these bones articulates anteriorly with the sphenotic and pterosphenoid, laterally with the pterotic, posteriorly with the exoccipital and basioccipital, and medially with the parasphenoid. The median parasphenoid extends along most of the basicranium. It is often broken and incomplete in the examined material, always lacking the paired posterior wings that extend posteriorly beyond the rear of the neurocranium in the extant *S. sagax* (Fig. 5A; see also Phillips, 1942; Svetovidov, 1952; Yabumoto, 1988; Matsuoka, 1997). The paired pterosphenoids and the median orbitosphenoid form the posterior and posterodorsal wall of the orbit together with the frontals.

Jaws and infraorbital bones are not recognizable in the examined material. Of the suspensorium, some badly preserved fragments of what appears to be a hyomandibula are preserved in MUSM 4730.

Of the opercular series, the opercle and subopercle can be observed in a few specimens (Fig. 6A). The opercle is large and trapezoid in outline. The dorsal margin is slightly oblique and the posterodorsal corner is rounded. The ventral margin is gently rounded and differs from that of the extant *S. sagax*, which is almost straight (e.g., Yabumoto, 1988). The anterior margin appears to be strongly thickened. There are several marked oblique bony striations in the anteroventral part of the opercle that radiate downward to reach the ventral margin of the bone. An incomplete subopercle is preserved in MUSM 4721, represented by a thick and flattened bony lamina showing an ornamented outer surface characterized by an irregular reticulate pattern (Fig. 6A).

The hyoid apparatus is not exposed in the available material, except for some fragments of the branchiostegal rays.

A largely incomplete articulated branchial skeleton can be recognized in MUSM 4730. It consists of incomplete, robust, rod-like bones, most likely the ceratobranchials and the epibranchials (see Nelson, 1967), which are associated with numerous, closely spaced and elongate gill rakers. These are thin, flattened, and distally pointed (Fig. 3F).

Some features of the axial skeleton can be defined thanks to incomplete articulated vertebral columns and isolated vertebrae. There is no evidence of the median and paired fins and girdles.

The vertebral number cannot be determined, although the abdominal vertebrae were certainly more than 17, as revealed by MUSM 4722 (Fig. 6B). The vertebral centra are rectangular, slightly longer than high, ornamented with thick longitudinal ridges separated from each other by grooves and fossae of variable size and depth. Robust parapohyses are partially preserved in certain vertebrae. Due to taphonomic compression, the neural and haemal spines are remarkably bent over those of the immediately posterior vertebrae. Dorsal and ventral prezygapophyses are well-developed, especially in the caudal vertebrae. The thick ribs are commonly fragmented. The epineurals insert at the level of the base of the neural arches; these are greatly elongate, especially those associated with the abdominal vertebrae, extending posteriorly for the length of about six vertebrae. The epicentrals are shorter, extending posteriorly for the length of three or four vertebrae. There are no complete epipleurals exposed in the examined material.

The structure and configuration of the caudal skeleton is largely recognizable in MUSM 4733 (Fig. 7); it consists of a large autogenous parhypural plus six autogenous hypurals, of which the second is fused with the first ural centrum; the

second ural centrum is almost rod-like; the first preural centrum is fused with a massive first uroneural and bears a neural spine of moderate size; the second uroneural is elongate and slender; the epurals are not preserved.

The scales are almost squared, with a gently curved posterior margin (Fig. 6E). There are subparallel grooves (fracture lines of Patterson et al., 2002), especially in the lateral fields, and tubercles are commonly present in the central portion of the scales.

One of the fragments pertaining to MUSM 4717 consists of a series of articulated abdominal scutes (Fig. 6D).

Distribution: Upper Miocene of Peru and Chile.

Discussion: Despite their incompleteness and fragmentary nature, the sardine remains described herein exhibit a set of morphological features that support their recognition as a new species of the alosid genus *Sardinops*. The presence of marked fronto-parietal striae on the outer surface of the skull roof, the well-developed and posteriorly directed spinous pterotic process, as well as the presence of bony striations radiating downward on the lateral surface of the opercle unambiguously support the placement of the fossils described herein within the family Alosidae (in the sense of Wang et al., 2022). The overall architecture of the neurocranium, oblique orientation of the marked opercular striations, and squared scales bearing subparallel grooves mostly in the lateral fields and tubercles in their central portion, justify the attribution to genus *Sardinops* (Fig. 5; see also Hubbs, 1929; Chapman, 1944; Svetovidov, 1952; Whitehead, 1985; Yabumoto, 1988; Patterson et al., 2002).

The genus *Sardinops* was established by Hubbs (1929) to separate the Indian-Pacific sardines from the European sardines of the genus *Sardina*. Several attempts to clarify the taxonomy of the *Sardinops* species have been carried out in the last century (e.g., Fowler, 1941; Hildebrand, 1946; Svetovidov, 1952; Ahlstrom, 1960), and some authors recognized five species to identify distinct populations widely separated geographically (e.g., Whitehead, 1985). However, the recognition of a single species, *Sardinops sagax*, is currently regarded as the best option (e.g., Parrish et al., 1989).

The fossils described herein are characterized by a unique neurocranial morphology that justifies their recognition as a previously unrecognized separate species of the genus *Sardinops*. In particular, as described above they show a set of features that clearly distinguish them from *Sardinops sagax*, including the possession of larger parietals and of thick and much elongate supraoccipital crest, anterolateral processes of the sphenotics that protrude obliquely rather than perpendicularly from the skull roof, posterior margins of the supraoccipital and epioccipitals forming a broad acute (versus obtuse) angle approaching 90°, and gently rounded ventral margin of the opercle.

Skeletal remains, mostly cranial, which can be referred to the new species described herein — *Sardinops humboldti* n. sp. — have been reported from the Miocene of Chile (Oyanadel-Urbina et al., 2021), as well as as stomach content and regurgitates of sharks and cetaceans from the Miocene of the Pisco Basin (Collareta et al., 2015, 2017; Lambert et al., 2015), tentatively referred to the extant *S. sagax*. In addition, the very abundant *Sardinops* scales commonly found in the sediments of the P1 and P2 sequences of the Pisco Formation (e.g., Collareta et al., 2021) most likely pertain to *S. humboldti* n. sp., as also does the indeterminate alosid reported by de Muizon and DeVries (1985) as widespread in the Neogene vertebrate levels of the Pisco-equivalent strata of the Sacaco area, further south along the Peruvian coast.

5. Taphonomy

Both the isolated and nodule-embedded sardine specimens are characterized by limited compression as well as by an excellent preservation of skeletal tissues, with scarce evidence of deformation and fine histological details that are still recognizable under transmitted light (Fig. 8A, B). The lithified sedimentary matrix filling the cavities of the isolated specimen and making up the nodule consists of a dominant biogenic fraction represented by diatom valves (which in some cases are unaffected by compaction) and subordinated sponge spicules, associated with a minor siliciclastic and volcanogenic fraction (Fig. 8D–G). SEM-EDS analyses of polished thin sections and freshly broken chips highlighted a Ca-P elemental composition (Fig. 8H, I) for both the bony elements and the mineral phase permeating the diatom valves and sediment porosity. This often occurs in the form of rod- or needle-like elements as typical of authigenic apatite (Fig. 8J–L).

Phosphogenesis is a recurrent process known from both modern and ancient upwelling systems (e.g., Bosio et al., 2024), where phosphorous is commonly sourced by decay-

Fig. 8. Photomicrographs and EDS maps of nodule-free and nodule-embedded specimens from the Upper Miocene of Las Antenas, Pisco Formation, Peru. (A–F) Transmitted light photomicrographs; (A) posterior portion of the neurocranium of *Sardinops humboldti* n. sp., showing limited evidence of deformation; (B) disarticulated, postcranial skeletal remains unaffected by compaction in the nodule-embedded specimen; (C) small-scale detail of bone in the nodule-free specimen, revealing the preservation of osteocyte lacunae and canaliculi-like structures (arrowheads); (D) osteocyte lacunae in the nodule-embedded specimen; (E) indurated sediment (central dashed line area) filling bone cavity (nodule-free specimen); (F) centric diatom frustule (arrowhead) unaffected by compaction, in the nodule-embedded specimen. (G–L) SEM photomicrographs and EDS maps; (G) centric diatom frustule unaffected by compaction, at the boundary with the bone (above the dashed line)in the nodule-embedded specimen; (H) EDS maps of nodule-free specimen; for sake of simplicity, besides Ca and P only Si — major constituent of the biogenic and terrigenous-volcanogenic fraction — is reported; (I) EDS map of a detail of nodule-embedded specimen; for sake of simplicity, besides Ca and P only Si — the major constituent of the biogenic and terrigenous-volcanogenic fraction — is reported; (J) diatom remains filled by authigenic apatite in the nodule-free specimen; (K) rod-shaped authigenic apatite filling the pores of a volcanic glass in the nodule-free specimen; (L) centric diatom valve almost filled with authigenic apatite in the nodule-embedded specimen.

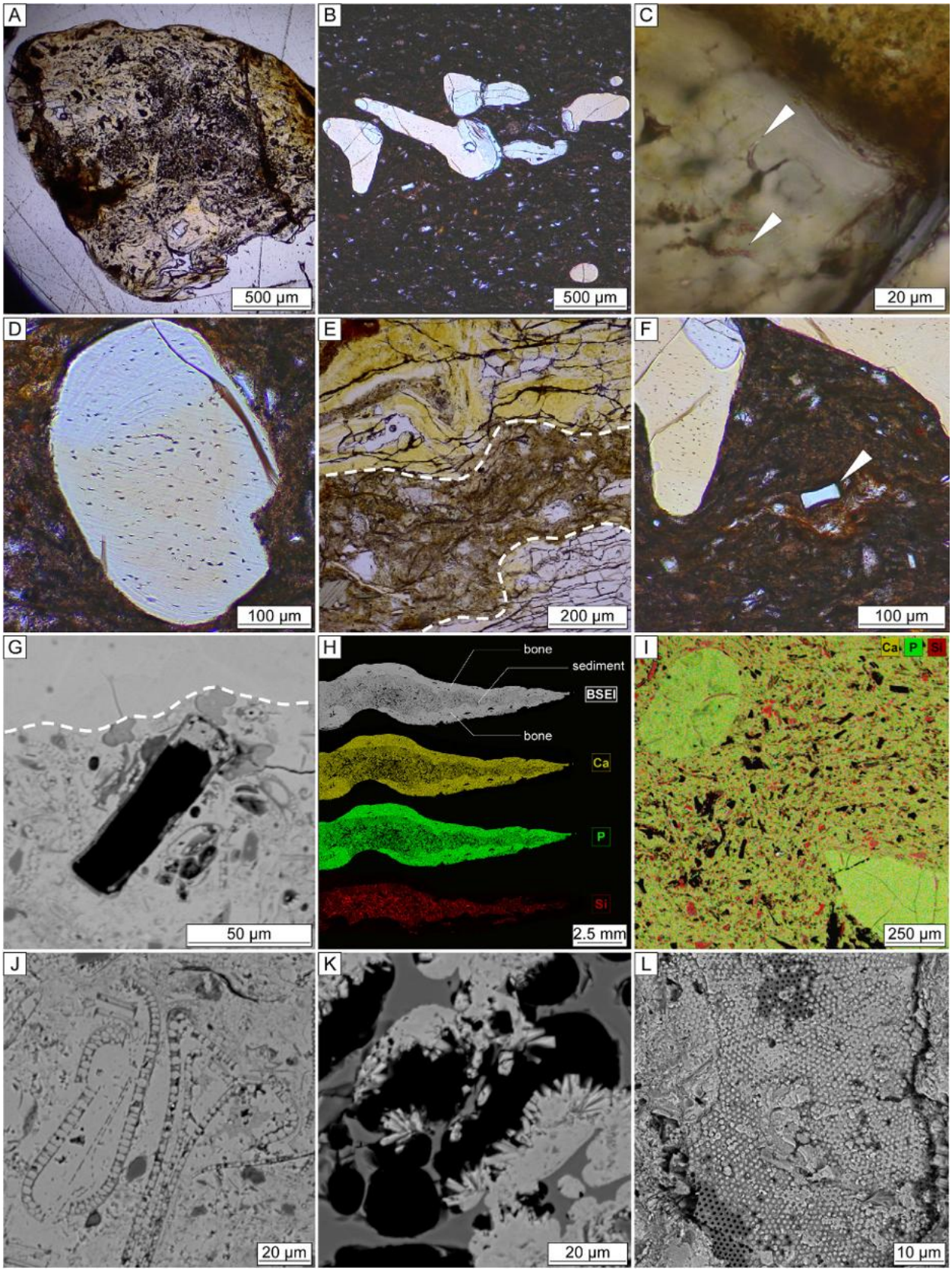
A
500 μm
B
500 μm
C
20 μm
D
100 μm
E
200 μm
F
100 μm
G
50 μm
H
bone
sediment
BSEI
bone
Ca
P
Si
2.5 mm
I
Ca
P
Si
250 μm
J
20 μm
K
20 μm
L
10 μm

ing phytoplankton and, occasionally, by vertebrate carcasses. The preservation of the sardine remains is indicative of a fast phosphatization of the bony tissues, which locally involved the surrounding diatomaceous sediment, leading to the formation of a hardened concretion. This early diagenetic process favored the limited deformation of the skeletal remains, as also witnessed by some pristinely preserved diatom valves recorded in the nodule. This kind of preservation largely differs from that characterizing most of the large cetacean skeletons from the Pisco Formation (Gariboldi et al., 2015). Moreover, dolomite and pyrite were not recorded in the examined specimens, thereby excluding the emergence of widespread organoclastic sulfate reduction (e.g., Gioncada et al., 2018). This is consistent with observations by Gariboldi et al. (2015), who regarded the amount of decaying organic matter (i.e. the carcass volume), as the main limiting factor for this bacterial degradative pathway that may result in increasing pore water alkalinity and promoting dolomite precipitation. In addition, no evidence of primary Mn-oxide precipitation has been observed in the examined sardine specimens, representing a further difference from the taphonomic model reported by Gioncada et al. (2018). However, it is reasonable to hypothesize that, although the immediate surroundings of the small sardine carcasses may have been somewhat oxygen-depleted, the bottom waters and the surrounding sediment were most likely fully oxygenated. Possibly, anoxic to suboxic conditions occurred within the sediment, well below the water-sediment interface, thereby limiting the migration of a substantial amount of reduced manganese to the redox boundary, which in turn would have precluded its precipitation in the form of Mn-oxyhydroxides around the carcasses.

The reason for the occurrence of nodule-free versus nodule-embedded specimens is less clear, especially considering that the former are almost invariably represented by neurocrania and partially articulated head bones, while the latter mostly consists of post-cranial remains. This can be possibly attributed to the detachment of neurocrania and head bones from the postcranium, leading to different preservation patterns. In this context, the nodule-free and nodule-embedded specimens occur within the same horizon albeit at different outcrops, thereby suggesting the influence of different local conditions at the seafloor and/or within the sediment.

6. Paleoecology

As reported above, the size of the neurocrania is consistent throughout the examined sample, as are those of the vertebrae and scales, thereby evidencing a substantial uniformity and size-specificity in the individual assemblage. This might reflect the structure and composition of the original schools formed by *Sardinops humboldti* n. sp. in the EPB during the Late Miocene. The size of the individuals within small sardine schools is remarkably uniform, indicating a sharp size-specificity in schooling behaviour (Blaxter and Hunter, 1982). Conversely, large clupeiform schools are not substantially uniform in size composition and commonly segregate internally by size due to the continuous adjustment in speed, interfish distance and headings that occur within the schools (e.g., Breder, 1976; Mužinić, 1977). However, the majority of the schools are small (less than 30 m long and less than 15 m thick; see Mais, 1974), especially during the foraging periods (Radakov, 1973). While the incompleteness of the available material does not allow to estimate the (total and/or standard) body length of the specimens, the size of their vertebral centra and of the scales is fully consistent with those of the specimens comprising the cetacean regurgitalite described by Lambert et al. (2015), whose average body length was estimated to be about 38.8 cm (with a standard deviation of 2.3 cm), with an average body weight of about 410 g (Lambert et al., 2015), thereby exceeding the average size of the extant Indian-Pacific sardine *Sardinops sagax* (especially that of the south-eastern Pacific populations; see Whitehead, 1985).

Based on the available evidence, therefore, it is reasonable to suggest that (relatively small) schools of *Sardinops humboldti* n. sp. formed by large individuals uniform in size commonly occurred in the EPB during the deposition of the Pisco Formation. Collareta et al. (2021) extensively discussed the ecological role of sardines in the EPB, evidencing their key role in the trophic web, and hypothesized that the Late Miocene strengthening of the Humboldt Current and the El Niño perturbations (see Gariboldi et al., 2023) promoted the flourishing of fast-growing planktonic organisms and sardines. The extant sardines of the genus *Sardinops* are particularly adapted for migration and are characterized by a very fine-meshed filtering apparatus in their gill rakers (van der Lingen, 1994) that allow them to feed primarily on small copepods and dinoflagellates (e.g., Espinoza et al., 2009). The very efficient filter feeding of *Sardinops* requires broad suitable vertical habitats, with a well oxygenated water column (both horizontally and vertically), moderate productivity, and a great concentration of small zooplankton (Bertrand et al., 2011). *Sardinops* populations increase in the eastern Pacific during El Niño conditions (Bakun and Broad, 2003), which favor the predomination of small zooplanktonic organisms (Bakun, 2006).

In summary, the Late Miocene marine ecosystem of the Pisco Basin was probably characterized by a "wasp-waist" structure (e.g., Cury et al., 2000; Bakun, 2006), in which a single species — namely, the planktivorous *S. humboldti* n. sp., entirely dominated its own trophic level, representing the trophic nucleus (see Carnevale et al., 2022) of the highly diverse vertebrate communities (Collareta et al., 2021). In this context, the *Sardinops* populations were probably strongly influenced by the variability of the physical ocean-atmosphere system that led to substantial demographic fluctuations of this planktivorous fish, thereby resulting in a remarkable variability of the trophic dynamics of the entire ecosystem. El Niño events likely promoted the development of environmental conditions favorable to

the increase of *Sardinops* populations that were associated with moderate abundance of diatoms (Gariboldi et al., 2023) and small zooplanktonic organisms.

7. Paleobiogeographic remarks

Sardines of the genus *Sardinops* are of considerable commercial importance today and together with anchovies, currently dominate the fish biomass of subtropical and temperate coastal upwelling systems as well as the temperate ecosystems influenced by the boundary currents in the Indian and Pacific oceans (e.g., Parrish et al., 1989). However, despite the remarkable abundance in the Indian and Pacific oceans today, the paleontological documentation of the past distribution of the genus *Sardinops* is very poor and largely inadequate to interpret its origin and evolutionary dynamics. The scarcity of fossil remains of *Sardinops* was noted by Fitch (1969). Fossil alosids exhibit a record that extends back to the Eocene, as documented by *Eoalosa janvieri* from the upper Ypresian laminated limestone of Bolca (Marramà and Carnevale, 2018). Genetic studies suggested that *Sardinops* originated in the Early Miocene, about 20 Ma, as a result of a vicariance event in response to the closure of the Tethyan Seaway (e.g., Parrish et al., 1989; Grant and Leslie, 1996; Bowen and Grant, 1997; Grant and Bowen, 1998). However, the earliest documented record of *Sardinops* dates back to the Bartonian, represented by a single otolith referred to *Sardinops* sp. from the Landrun Member, Texas (Lin and Nolf, 2022). In addition, a late Oligocene otolith-based species, *Sardinops robinsoni*, was described from the Chatton Formation, New Zealand by Schwarzhans et al. (2017). Parrish et al. (1989) suggested that *Sardinops* achieved its present distribution during the Late Miocene. Such hypothesis fits remarkably well with the record from the Pisco Basin described herein, and with the fossil vertebra from the Upper Miocene Wilson Cove Formation, California, reported by Powell II et al. (2019). The occurrence of *Sardinops* in the northwestern Pacific is documented at least since the Pliocene by otoliths from the Dainichi Sands in Japan (Takahashi, 1977). Finally, the origin of the extant species *Sardinops sagax* can be traced back to the Pleistocene, with a record consisting of both otoliths and skeletal remains (e.g., Aoki, 1968; Yabumoto, 1988).

Declaration of competing interest

The authors declare that they have no known competing financial interests or personal relationships that could have appeared to influence the work reported in this paper.

Acknowledgments

Our thanks go to Rodolfo Salas-Gismondi and Alí Altamirano Sierra for laboratory assistance and fruitful discussions, and to Rafael Varas-Malca for support during field work. Research is supported by the European Union – NextGenerationEU, Mission 4, Component 2 CUP I53D23002070 006, project title: BIOVERTICES (BIOdiversity of VERTebrates In the CEnozoic Sea). The manuscript has benefited from the comments and suggestions made by two anonymous reviewers.

References

Ahlstrom, E.H., 1960. Synopsis on the biology of the Pacific sardine (*Sardinops cearulea*). In: Proceedings of the World Scientific Meeting on the Biology of the Sardines and Related Species. Vol. 2. FAO, Rome, pp. 415–451.

Aoki, N., 1968. Some Pleistocene fish-otoliths from the Boso and Miura Peninsulas. Transactions of the Paleontological Society of Japan 71, 296–307.

Bakun, A., 2006. Wasp-waist populations and marine ecosystem dynamics: navigating the "predator pit" topographies. Progress in Oceanography 68, 271–288.

Bakun, A., Broad, K., 2003. Environmental 'loopholes' and fish population dynamics: comparative pattern recognition with focus on El Niño effects in the Pacific. Fisheries Oceanography 12, 458–473.

Bertrand, A., Chaigneau, A., Peraltilla, S., Ledesma, J., Graco, M., Monetti, F., Chavez, F.P., 2011. Oxygen: A fundamental property regulating pelagic ecosystem structure in the coastal southeastern tropical Pacific. PLoS ONE 6, e29558.

Bianucci, G., Collareta, A., 2022. An overview of the fossil record of cetaceans from the East Pisco Basin (Peru). Bollettino della Società Paleontologica Italiana 61, 19–60.

Bianucci, G., Di Celma, C., Collareta, A., Landini, W., Post, K., Tinelli, C., de Muizon, C., Bosio, G., Gariboldi, K., Gioncada, A., Malinverno, E., Cantalamessa, G., Altamirano-Sierra, A., Salas-Gismondi, R., Urbina, M., Lambert, O., 2016. Fossil marine vertebrates of Cerro Los Quesos: Distribution of cetaceans, seals, crocodiles, seabirds, sharks, and bony fish in a late Miocene locality of the Pisco Basin, Peru. Journal of Maps 12, 1037–1046.

Blaxter, J.H.S., Hunter, J.R., 1982. The biology of clupeoid fishes. Advances in Marine Biology 20, 1–223.

Bleeker, P., 1859. Enumeratio specierum piscium hucusque in Archipelago indico observatarum, adjectis habitationibus citationibusque, ubi descriptiones earum recentiores reperiuntur, nec non speciebus Musei Bleekeriani Bengalensibus, Japonicis, Capensibus Tasmanicisque. Acta Societatis Regiae Scientiarum Indo-Neêrlandicae 6, 1–276.

Bosio, G., Collareta, A., Di Celma, C., Lambert, O., Marx, F.G., de Muizon, C., Gioncada, A., Gariboldi, K., Malinverno, E., Varas Malca, R., Urbina, M., Bianucci, G., 2021. Taphonomy of marine vertebrates of the Pisco Formation (Miocene, Peru): Insights into the origin of an outstanding Fossil-Lagerstätte. PLoS ONE 16, e0254395.

Bosio, G., Gioncada, A., Malinverno, E., Coletti, G., Collareta, A., Mariani, L., Cavallo, A., BIanucci, G., Urbina, M., Di Celma, C., 2024. Unraveling marine phosphogenesis along the Miocene coast of Peru: Origin and sedimentological significance of the Pisco Formation phosphorites. Marine and Petroleum Geology 167, 106941.

Bowen, B.W., Grant, W.S., 1997. Phylogeography of the sardines (*Sardinops* spp.): Assessing biogeographic models and populations histories in temperate upwelling zones. Evolution 51, 1601–1610.

Breder, C.M., 1976. Fish schools as operational structures. Fishery Bulletin 74, 471–502.

Carnevale, G., Pellegrino, L., Natalicchio, M., Dela Pierre, F., 2022. The Messinian fishes of Capo di Fiume (Palena, Abruzzo): Stratigraphy, taphonomy and paleoecology. Bollettino della Società Paleontologica Italiana 61, 91–118.

Chapman, W.M., 1944. The comparative osteology of the herring-like fishes (Clupeidae) of California. California Fish and Game 30, 6–21.

Clift, P.D., Vannucchi, P., 2004. Controls on tectonic accretion versus erosion in subduction zones: implications for the origin and recycling of the continental crust. Reviews of Geophysics 42, 2003RG000127.

Collareta, A., Landini, W., Lambert, O., Post, K., Tinelli, C., Di Celma, C., Panetta, D., Tripodi, M., Salvadori, P.A., Caramella, D., Marchi, D., Urbina, M., Bianucci, G., 2015. Piscivory in a Miocene Cetotheriidae of Peru: first record of fossilized stomach content for an extinct baleen-bearing whale. The Science of Nature 102, 70.

Collareta, A., Landini, W., Chacaltana, C., Valdivia, W., Altamirano Sierra, A., Urbina Schmitt, M., Bianucci, G., 2017. A well preserved skeleton of the fossil shark *Cosmopolitodus hastalis* from the late Miocene of Peru, featuring fish remains as fossilized stomach contents. Rivista Italiana di Paleontologia e Stratigrafia 123, 11–22.

Collareta, A., Lambert, O., Marx, F.G., de Muizon, C., Varas-Malca, R., Landini, W., Bosio, G., Malinverno, E., Gariboldi, K., Gioncada, A., Urbina, M., Bianucci, G., 2021. Vertebrate paleoecology of the Pisco Formation (Miocene, Peru): Glimpses into the ancient Humboldt Current ecosystem. Journal of Marine Science and Engineering 9, 1188.

Cury, P., Bakun, A., Crawford, R.J.M., Jarre-Teichmann, A., Quiñones, R.A., Shannon, L.J., Verheye, H.M., 2000. Small pelagics in upwelling systems: patterns of interaction and structural changes in "wasp-waist" ecosystems. ICES Journal of Marine Science 210, 603–618.

de Muizon, C., DeVries, T.J., 1985. Geology and paleontology of late Cenozoic marine deposits in the Sacaco area (Peru). Geologische Rundschau 74, 547–563.

Di Celma, C., Pierantoni, P.P., Volatili, T., Molli, G., Mazzoli, S., Sarti, G., Ciattoni, S., Bosio, G., Malinverno, E., Collareta, A., Gariboldi, K., Gioncada, A., Jablonská, D., Landini, W., Urbina, M., Bianucci, G., 2022. Towards deciphering the Cenozoic evolution of the East Pisco basin (southern Peru). Journal of Maps 18, 397–412.

Dunbar, R.B., Marty, R.C., Baker, P.A., 1990. Cenozoic marine sedimentation in the Sechura and Pisco basins, Peru. Palaeogeography, Palaeoclimatology, Palaeoecology 77, 235–261.

Espinoza, P., Bertrand, A., van der Lingen, C.D., Garrido, S., de Mendiola, B.R., 2009. Diet of sardine (*Sardinops sagax*) in the northern Humboldt Current system and comparison with the diets of clupeoids in this and other eastern boundary upwelling systems. Progress in Oceanography 83, 242–250.

Fitch, J.E., 1969. Fossil records of certain schooling fishes of the California Current System. California Marine Research Commission, CalCOFI Reports 13, 71–80.

Fowler, H.W., 1941. Contributions to the biology of the Philippine Archipelago and adjacent regione. The fishes of the groups Elasmobranchii, Holocephali, Isospondyli, and Ostariophysi obtained by the United States Bureau of Fisheries steamer "Albatross" in 1907 to 1910, chiefly in the Philippine Islands and adjacent seas. Bulletin of the United States National Museum 100, 620–625.

Gariboldi, K., Gioncada, A., Bosio, G., Malinverno, E., Di Celma, C., Tinelli, C., Cantalamessa, G., Landini, W., Urbina, M., Bianucci, G., 2015. The dolomite nodules enclosing fossil marine vertebrates in the East Pisco Basin, Peru: field and petrographic insights into their genesis and role in preservation. Palaeogeography, Palaeoclimatology, Palaeoecology 438, 81–95.

Gariboldi, K., Pike, J., Malinverno, E., Di Celma, C., Gioncada, A., Bianucci, G., 2023. Paleocenographic implications of diatom seasonal laminations in the Upper Miocene Pisco Formation (Ica Desert, Peru) and their clues on the development of the Pisco Fossil-Lagerstätte. Paleoceanography and Paleoclimatology 38, e2022PA004566.

Gioncada, A., Gariboldi, K., Collareta, A., Di Celma, C., Bosio, G., Malinverno, E., Lambert, O., Pike, J., Urbina, M., Bianucci, G., 2018. Looking for the key to preservation of fossil marine vertebrates in the Pisco Formation of Peru: new insights from a small dolphin skeleton. Andean Geology 45 (3), 379–398.

Grant, W.S., Bowen, B.W., 1998. Shallow population histories in deep evolutionary lineages of marine fishes: Insights from sardines and anchovies and lessons for conservation. Journal of Heredity 89, 415–426.

Grant, W.S., Leslie, R.W., 1996. Late Pleistocene dispersal of Indian-Pacific sardine populations in an ancient lineage of the genus *Sardinops*. Marine Biology 126, 133–142.

Herbozo, G., Kukowski, N., Clift, P.D., Pecher, I., Bolaños, R., 2020. Cenozoic increase in subduction erosion during plate convergence variability along the convergent margin off Trujillo, Peru. Tectonophysics 790, 228557.

Hildebrand, S.F., 1946. A descriptive catalog of the shore fishes of Peru. Bulletin of the United States National Museum 189, 1–530.

Hsu, J.T., 1992. Quaternary uplift of the Peruvian coast related to the subduction of the Nazca Ridge: 13.5 to 15.6 degrees south latitude. Quaternary International 15, 87–97.

Hubbs, C.L., 1929. The generic relationships and nomenclature of the California sardine. Proceedings of the California Academy of Sciences 18, 261–265.

Lambert, O., Collareta, A., Landini, W., Post, K., Ramassamy, B., Di Celma, C., Urbina, M., Bianucci, G., 2015. No deep diving: evidence of predation on epipelagic fish for a stem beaked whale from the Late Miocene of Peru. Proceedings of the Royal Society B: Biological Sciences 282, 20151530.

Lin, C.H., Nolf, D., 2022. Middle and late Eocene fish otoliths from the eastern and southern USA. European Journal of Taxonomy 84, 1–122.

Macharé, J., Ortlieb, L., 1992. Plio-Quaternary vertical motions and the subduction of the Nazca Ridge, central coast of Peru. Tectonophysics 205, 97–108.

Mais, K.F., 1974. Pelagic fish surveys in the California Current. California Fish and Game, Fish Bulletin 162, 1–79.

Marramà, G., Carnevale, G., 2018. *Eoalosa janvieri* gen. et sp. nov., a new clupeid fish (Teleostei, Clupeiformes) from the Eocene of Monte Bolca. Paläontologische Zeitschrift 92, 107–120.

Matsuoka, M., 1997. Osteological development in the Japanese sardine, *Sardinops melanostichus*. Ichthyological Research 44, 275–295.

Mužinić, R., 1977. On the shoaling of sardines (*Sardina pilchardus*) in aquaria. Journal du Conseil International pour l'Exploration de la Mer 37, 147–155.

Nelson, G.J., 1967. Gill arches of teleostean fishes of the family Clupeidae. Copeia 1967, 389–399.

Noda, A., 2016. Forearc basins: types, geometries, and relationships to subduction zone dynamics. Geological Society of America Bulletin 128, 879–895.

O'Connell, C., 1955. The gas bladder and its relation to the inner ear in *Sardinops caerulea* and *Engraulis mordax*. Fishery Bulletin 56, 503–533.

Oyanadel-Urbina, P., De Gracia, C., Carrillo-Briceño, J.D., Nielsen, S.N., Flores, H., Casteletto, V., Kriwet, J., Rivadeneira, M.M., Villafaña, J. A., 2021. Neogene bony fishes from the Bahía Inglesa Formation, Northern Chile. Ameghiniana 58, 345–368.

Parrish, R.H., Serra, R., Grant, W.S., 1989. The monotypic sardines, *Sardina* and *Sardinops*: their taxonomy, distribution, stock structure, and zoogeography. Canadian Journal of Fisheries and Aquatic Science 46, 2019–2036.

Patterson, R.T., Wright, C., Chang, A.S., Taylor, L.A., Lyons, P.D., Dallimore, A., Kumar, A., 2002. Atlas of common squamatological (fish scale) material in coastal British Columbia and an assessment of the utility of various scale types in paleofisheries reconstruction. Palaeontologia Electronica 4, 1–88.

Phillips, J.B., 1942. Osteology of the sardine (*Sardinops caerulea*). Journal of Morphology 70, 463–500.

Powell II, C.L., Boessenecker, R.W., Smith, N.A., Fleck, R.J., Carlson, S.J., Allen, J.R., Long, D.J., Sarna-Wojcicki, A.M., Guruswami-Naidu, R.B., 2019. Geology and paleontology of the late Miocene Wilson Grove Formation at Bloomfield Quarry, Sonoma County, California. U.S. Geological Survey Scientific Investigations Report 2019-5021, 1–77.

Radakov, D.V., 1973. Schooling in the Ecology of Fish. Wiley, New York, 174 pp.

Romero, D., Valencia, K., Alarcón, P., Peña, D., Ramos, V.A., 2013. The offshore basement of Peru: evidence for different igneous and metamorphic domains in the forearc. Journal of South America Earth Sciences 42, 47–60.

Schwarzhans, W., Lee, D.E., Gard, H.J.L., 2017. Otoliths reveal diverse fish communities in Late Oligocene estuarine to deep-water paleoen-

vironments in southern Zelandia. New Zealand Journal of Geology and Geophysics 60, 433–464.
Segura, V., Díaz de Astarloa, J., 2004. Análisis osteológico de la saraca *Brevoortia aurea* (Spix) (Actinopterygii: Clupeidae) en el Atlántico suroccidental. Revista de Biología Marina y Oceanografia 39, 37–52.
Svetovidov, A.N., 1952. Clupeidae. Fauna of the U.S.S.R., Fishes, Vol. 2, No. 1. Zoological Institute, Akademii Nauk SSR, St. Petersburg, 428 pp.
Svetovidov, A.N., 1964. Systematics of the North American anadromous clupeoid fishes of the genera *Alosa*, *Caspialosa*, and *Pomolobus*. Copeia 1964, 118–130.
Takahashi, M., 1977. Some Pliocene fish otoliths from the Dainichi sands, Kakegawa Group, Central Japan. Bulletin of the Mizunami Fossil Museum 4, 97–118.
Tejada, L., Chacaltana, C., Morales, M.D.C., Valdivia, W., 2010. Análisis preliminar de diatomeas en el cerro Pileta: Borde oriental de la Cuenca Pisco. XV Congreso Peruano de Geología. Resúmenes Extendidos. Publicaciones de la Sociedad Geológica del Perú 9, 245–248.
van der Lingen, C.D., 1994. Effect of particle size and concentration on the feeding behavior of adult pilchard, *Sardinops sagax*. Marine Ecology Progress Series 119, 1–13.
von Huene, R., Suess, E., 1988. Ocean drilling program Leg 112, Peru continental margin. Geology 16, 934–938.
Wang, Q., Dizaj, L.P., Huang, J., Sarker, K.K., Kevrekidis, C., Reichenbacher, B., Esmaeili, H.R., Straube, N., Moritz, T., Li, C., 2022. Molecular phylogenetics of the Clupeiformes based on exon-capture data and a new classification of the order. Molecular Phylogenetics and Evolution 175, 107590.
Whitehead, P.J.P., 1985. Clupeid fishes of the world. An annotated and illustrated catalogue of the herrings, sardines, pilchards, sprats, shads, anchovies and wolf-herrings. Part 1 – Chirocentridae, Clupeidae and Pristigasteridae. FAO Fisheries Synopsis 125, 1–303.
Yabumoto, Y., 1988. Pleistocene clupeid and engraulidid fishes from the Kokubu Group in Kagoshima Prefecture, Japan. Bulletin of the Kitakyushu Museum of Natural History 8, 55–74.